

COMPARISON BETWEEN AERODYNAMIC FORCE ON C AND H MESHES WITH NORMALIZED VARIABLE DIAGRAM

M.H. Djavareshkian, M. Salim-mokri
Mechanical Engineering Department,
University of Tabriz, Tabriz, Iran

ABSTRACT

In this paper, a pressure-based finite volume procedure is developed in an aerodynamic flow simulation on C- mesh. The boundedness criteria for this procedure are determined from the SBIC, Second and Blending Interpolation Combine, scheme which are used to solve the Euler equations on a nonorthogonal mesh. The results of this scheme on C and H meshes are compared with another numerical solution and experiment data for the cases of inviscid transonic flow around airfoil NACA0012.

KEYWORDS

Transonic flow, Normalized Variable Diagram, SBIC, Pressure-based, Aerodynamic coefficients

INTRODUCTION

Leonard⁽¹⁾ has generalized the formulation of the high-resolution flux limiter schemes using what is called the normalized variable formulation (NVF). The NVF methodology has provided a good framework for development of high-resolution schemes that combine simplicity of implementation with high accuracy and boundedness. Gaskell and Lau⁽²⁾ introduced SMART scheme that is combined with first and high order interpolation procedures based on NVD. The SFCD scheme was represented by Ziman⁽³⁾. Zhu and Rodi⁽⁴⁾ introduced SOUCUP scheme. Darwish⁽⁵⁾ developed STOIC scheme that is integrated from high order interpolation procedure to control convective term.

Most of NVD methods use different differencing schemes through the solution domain. This procedure includes some kind of switching between the differencing schemes. Switching introduced additional non-linearity and instability in to the computation. The worst case is that instead of a single solution for steady state problem, the differencing scheme creates two or more unconverged solution with the cyclic switching between them. In that case it is impossible to obtain a converged solution and convergence stalls at some level. The SBIC scheme was introduced by Javareshkian⁽⁶⁾ ; it is integrated from central interpolation and first and second order interpolation procedures.

The objective of this paper is to develop the SBIC scheme in C-mesh and to compare the results of the SBIC scheme in the context of an existing finite-volume procedure that uses C and H meshes and an implicit solver, to solve the Euler equations utilizing the pressure correction type of solution algorithm for calculation of external transonic flow.

GOVERNING EQUATIONS

The basic equations, which describe conservation of mass, momentum and scalar quantities, can be expressed in Cartesian tensor form as

$$\frac{\partial \rho}{\partial t} + \frac{\partial (\rho u_j)}{\partial x_j} = 0 \quad (1)$$

$$\frac{\partial (\rho u_i)}{\partial t} + \frac{\partial (\rho u_i u_j - T_{ij})}{\partial x_j} = S_i^u \quad (2)$$

$$\frac{\partial (\rho \phi)}{\partial t} + \frac{\partial (\rho u_j \phi - q_j)}{\partial x_j} = S^\phi \quad (3)$$

The stress tensor and scalar flux vector are usually expressed in terms of basic dependent variable. The stress tensor for a Newtonian fluid is

$$T_{ij} = -p \delta_{ij} - \frac{2}{3} \mu \frac{\partial u_k}{\partial x_k} \delta_{ij} + \mu \left(\frac{\partial u_i}{\partial x_j} + \frac{\partial u_j}{\partial x_i} \right) \quad (4)$$

The scalar flux vector usually given by the Fourier-type law:

$$q_j = \Gamma_\phi \left(\frac{\partial \phi}{\partial x_j} \right) \quad (5)$$

DISCRETIZATION

The discretization of the above differential equations is carried out using a finite-volume approach. First, the solution domain is divided into a finite number of discrete volumes or cells, where all variables are stored at their geometric centers (see e.g. Fig.1). The equations are then integrated over all the control volumes by using the Gaussian theorem. The discrete expressions are presented affected with reference to only one face of the control volume, namely, e , for the sake of brevity.

For any variable ϕ (which may also stand for the velocity components), the result of the integration yields

$$\frac{\delta v}{\delta t} [(\rho \phi)_p^{n+1} - (\rho \phi)_p^n] + I_e - I_w + I_n - I_s = S_\phi \delta v \quad (6)$$

where I 's are the combined cell-face convection I^c and diffusion I^D fluxes. The diffusion flux is approximated by central differences and can be written for cell-face e of the control volume in Fig. (1) as:

$$I_e^D = D_e(\phi_p - \phi_E) - S_e^\phi \quad (7)$$

where S_e^ϕ stands for cross derivative arising from mesh nonorthogonality. The discretization of the convective flux, however, requires special attention and is the subject of the various schemes developed. A representation of the convective flux for cell-face e is:

$$I_e^c = (\rho.V.A)_e \phi_e = F_e \phi_e \quad (8)$$

the value of ϕ_e is not known and should be estimated by interpolation, from the values at neighboring grid points. The expression for the ϕ_e is determined by the SBIC scheme, that is based on the NVD technique, used for interpolation from the nodes E, P and W. The expression can be written as

$$\phi_e = \phi_W + (\phi_E - \phi_W) \tilde{\phi}_e \quad (9)$$

the functional relationship used in SBIC⁽⁶⁾ scheme for $\tilde{\phi}_e$ is illustrated in Fig.2 and is given by:

$$\begin{aligned} \tilde{\phi}_e &= \tilde{\phi}_p & \text{if } \tilde{\phi}_p \notin [0,1] \\ \tilde{\phi}_e &= -\frac{\tilde{x}_p - \tilde{x}_e}{K(\tilde{x}_p - 1)} \tilde{\phi}_p^2 + \left(1 + \frac{\tilde{x}_p - \tilde{x}_e}{K(\tilde{x}_p - 1)}\right) \tilde{\phi}_p & \text{if } \tilde{\phi}_p \in [0, K] \\ \tilde{\phi}_e &= \frac{\tilde{x}_p - \tilde{x}_e}{\tilde{x}_p - 1} + \frac{\tilde{x}_e - 1}{\tilde{x}_p - 1} \tilde{\phi}_p & \text{if } \tilde{\phi}_p \in [0, K] \quad 0 \leq K \leq 0.5 \end{aligned} \quad (10)$$

where

$$\tilde{\phi}_p = \frac{\phi_p - \phi_W}{\phi_E - \phi_W} \quad \tilde{\phi}_e = \frac{\phi_e - \phi_W}{\phi_E - \phi_W} \quad \tilde{x}_e = \frac{x_e - x_W}{x_E - x_W} \quad \tilde{x}_p = \frac{x_p - x_W}{x_E - x_W}$$

the limits on the selection of K could be determined in the following way. Obviously the lower limit is $K = 0$, which would represent switching between upwind and central differencing. This is not favorable because; it is essential to avoid the abrupt switching between the schemes in order to achieve the converged solution. The value of K should be kept as low as possible in order to achieve the maximum resolution of the scheme.

With higher-order schemes, the evaluation of ϕ_e may involve a large number of neighboring grid points. Therefore, in order to simplify the solution of the resulting system of algebraic equations, a compacting procedure is usually used. The deferred correction procedure of Rubin and Khosla⁽⁷⁾ adapted in this work, is based on replacing the convective flux at control volume face by an equivalent flux given by

$$I_e^c = F_e \phi_e = F_e \phi_e^U - F_e (\phi_e^U - \phi_e)$$

where the superscript U denotes values obtained by the first-order upwind scheme, and ϕ_e represents cell face value computed by SBIC scheme. With the preceding assumption, each discretized equation contains five unknowns (in two dimensions), and the matrix of coefficients of the resulting system of equations is pentadiagonal and always diagonally dominates since it is formed using the first order upwind scheme. The final form of the discretized equation from each approximation is given as:

$$A_p \cdot \phi_p = \sum_{m=E,W,N,S} A_m \cdot \phi_m + S'_\phi + S_{dc} \quad (11)$$

where A 's are the convection-diffusion coefficients. The term S'_ϕ in Eq. (11) contains quantities arising from non-orthogonality, numerical dissipation terms and external sources, and $(\rho \delta v / \delta t) \phi_p$ of the old time-step/iteration level (for time dependent equation). For the momentum equations it is easy to separate out the pressure-gradient source from the convected momentum fluxes. S_{dc} is the contribution due to the adapted deferred correction procedure.

SOLUTION ALGORITHM

Most contemporary pressure-based methods employ a sequential iteration technique in which the different conservation equations are solved one after another. The common approach taken in enforcing continuity is by combining the equation for continuity with those of momentum to derive an equation for pressure or pressure-correction. The PISO algorithm is used in this work.

RESULTS

Computational results are shown in followed figures for a baseline series of test cases. The results are compared with existing numerical solutions obtained by others. Figure 5 displays part of the C and H grids used for the present computation. The value of K in SBIC method for all cases is 0.2 .

The first case considered is transonic flow around an NACA 0012 airfoil at a freestream mach number of $M=0.85$, angle of attack $\alpha=0$ deg. The far-field boundary placed at 17 chord lengths away from the airfoil surface and 20 chord lengths away from the leading and trailing edges for H grid and a grid with 116×149 nodes is used in this test. For C grid, the far-field boundary placed at 15 chord lengths away from the airfoil surface and a grid with 500×80 nodes is used. The distribution of pressure coefficients on the upper surface of airfoil for C and H meshes and contours of pressure coefficient are shown in Figure 6(a) and 6(b) respectively. The present results are compared with those of Jameson and Yoon⁽⁸⁾ . It can be seen that the computed results show good agreement. A sharp discontinuity is achieved successfully for both shock strength and location and the mesh is not so effect on the results. Also aerodynamic coefficients for this case are presented in table 1. Accuracy of these coefficients is good.

The second case is transonic flow around NACA0012 airfoil at $M=0.85$, $\alpha=1$ deg and a 150×149 nodes for H grid. The number of nodes for the C grid is the same of previous case. For this case distribution of pressure coefficient on the upper and lower surface of airfoil for C and H meshes and contours of pressure coefficient are shown in Figures 7(a) and 7(b) respectively. The results are compared with those of Zhou⁽⁹⁾ . Also aerodynamic coefficients for this case are presented in table 2. The results of the SBIC scheme with H mesh show that the lower surface shocks are captured better than C-grid. Third case is for $M=0.8$, $\alpha=1.25$ deg and with the same previous grid for C and H meshes. The distribution of pressure coefficient on the upper and lower surface of airfoil

and contours of pressure coefficient are shown in Figures 8(a) , 8(b) . In this case results are compared with those of Anderson⁽¹⁰⁾. Also aerodynamic coefficients for this case are presented in table 3. It can be seen that the results (especially shock gradients) of the SBIC scheme with H mesh are better than the result of this scheme with C-mesh.

CONCLUSION

In this paper, the SBIC scheme has been developed in the context of an existing finite-volume procedure that uses nonorthogonal C mesh, and a pressure correction type of solution algorithm for accurate simulation of external transonic compressible inviscid flows. The results of the proposed algorithm with C and H meshes are compared with another published results. These comparison show although simulation with H mesh take more than time but the results of SBIC scheme on H-mesh are more accurate. Also the agreement between the results of the present work with another numerical and experimental data is remarkable.

REFERENCES

- [1] Leonard B.P., 1988, “ Simple High-Accuracy Resolution Program for convective modeling of discontinuities”, *International Journal for Numerical Methods in Fluids*, Vol.8, pp.1291-1318
- [2] Gaskell P.H. & Lau A.K.C. ,1988, “Curvature-Compensated convective Transport: SMART, a new boundedness-preserving transport algorithm”, *International Journal for Numerical Methods in Fluid*, Vol.8, pp.617-641
- [3] Ziman H., 1991, *A Computer Prediction of Chemically Reacting Flows in Stirred Tanks*”, PhD thesis, University of London
- [4] Zhu J. & Rodi W. ,1991, “A Low Dispersion and Bounded Convection Scheme”, *Computer Methods in Applied Mechanics and Engineering*, Vol. 92, pp.87-96
- [5] Darwish M.S. ,1993, “A New High-Resolution Scheme based on the normalize variable Formulation”, *Numerical Heat Transfer*, Part B, Vol.24, pp.353-371
- [6] Javareshkian, M. H, 2004, Pressure-Based Compressible Calculation Method Utilizing Normalized variable D \ddot{a} gram Scheme, *Iranian Journal of Science and Technology*, Transaction B, Vol. 28, No. B4, Sept, 2004, PP. 495-500
- [7] Rubin S.G. and Khosla P.K.,1982, Polynomial Interpolation Method for Viscous Flow Calculations, *J. Comput. Phys.*, Vol.27, pp.153-168
- [8] Rizzi, A. Spurious Entropy and Very Accurate Solutions to Euler Equations.,1984, *AIAA Paper*, 84 –1644.
- [9] Zhou, G. and Davidson, L.,1995, A Pressure Based Euler Scheme for Transonic Internal and External flow Simulation . *Int. J. Comp. Fluid Dynamics*, Vol. 5, No. 3-4: 169 - 188.
- [10] Anderson, W. K. and James, L. T.,1986, Comparison of Finite Volume Flux Vector Splittings for the Euler Equations. *AIAA Journal*, Vol. 24, No. 9: 1453 – 1460 .
- [11]- Javareshkian, M. H & Baheri Islami S.,2004, Transonic Turbulent Flow Simulation Using Pressure-Based Method And Normalized Variable Diagram, *International Journal of Engineering, Transactions B*, Vol. 17, No. 3, October 2004

- [12] Pulliam, T. H., and Barton, J. T, 1985, “Euler Computations of AGARD Working 07 Airfoil Test Cases”, AIAA Paper: 85-0018.
- [13] Dervieux, A., and Debiez, C.,1996, “Application of Mixed Element-Volume Muscl Method with 6th Order Viscosity Stabilization to Steady and unsteady Flow Calculation. Proceeding of Computational Fluid Dynamics”. John Wiley & Sons Ltd.
- [14] Jameson,1998, A., and Martinelli, L. “Mesh Refinement and Modeling Errors in Flow Simulation”. *AIAA J.*, Vol.36, No.5.
- [15] Caughey, D. A.,1988, “Diagonal Implicit Multigrid Algorithm for Euler Equations”, *AIAA J.*, Vol.26, No.7, pp. 841-851..

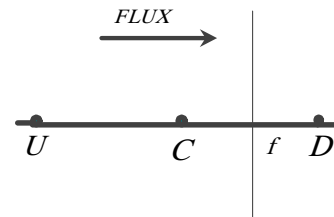
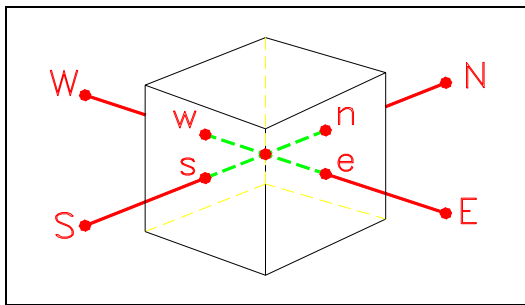


Figure 1- Typical grid – point cluster and control volume

Figure 2- Node value in the normalized variable approach

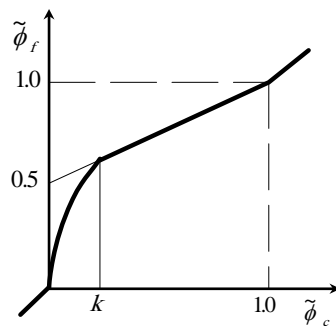


Figure 4 – Normalized variable diagram (NVD)or SBIC scheme

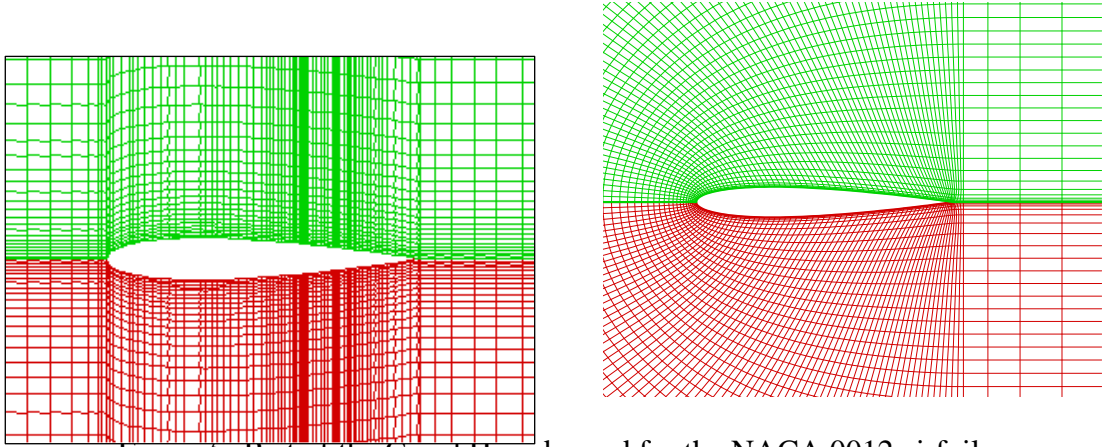
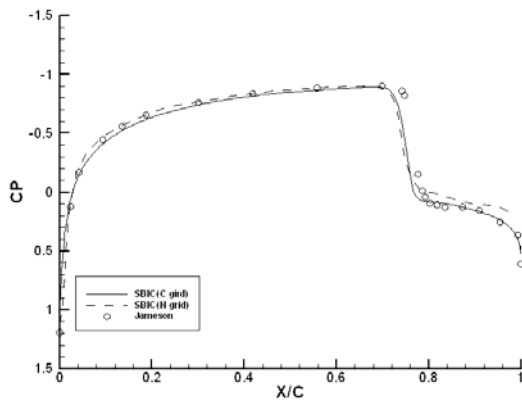
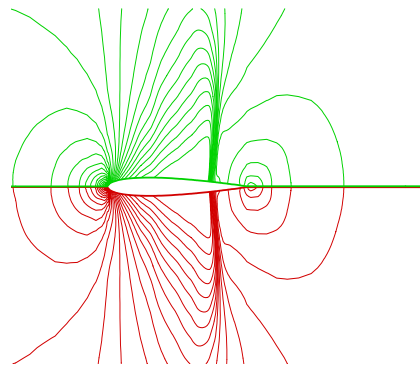


Figure 5- Part of the C and H grids used for the NACA 0012 airfoil

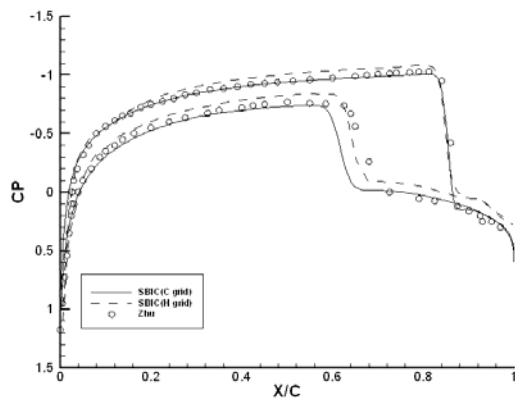


(a)

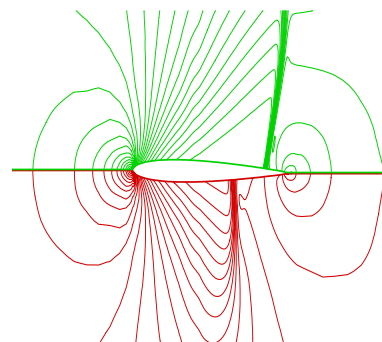


(b)

Figure 6–(a) Surface pressure coefficient distribution (b) Pressure coefficient contours for $\alpha=0$ and $M=0.85$



(a)



(b)

Figure 7-(a) Surface pressure coefficient distribution (b) Pressure coefficient contours for $\alpha=1$ and $M=0.85$.

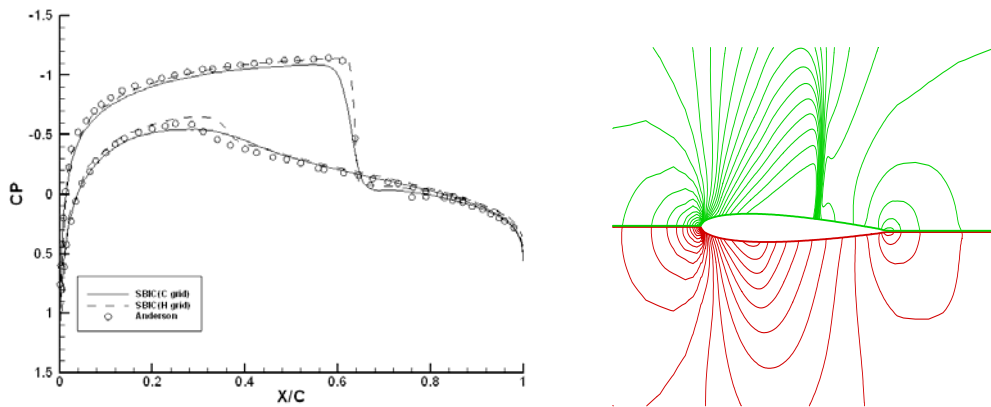


Figure 8-(a) Surface pressure coefficient distribution (b) Pressure coefficient contours for $\alpha=1.25$ and $M=0.8$.

Table 1. Aerodynamic coefficients NACA0012: $M = 0.85$, $\alpha = 0$

Method	C_L	C_D	C_M
Rizzi[8]	0	0.0471	0
Zhou & Davidson[9]	0	0.0559	0
SBIC(C grid)	-0.002	0.047	0.001
SBIC(H grid)[11]	0	0.049	0

Table 2. Aerodynamic coefficients NACA0012: $M = 0.85$, $\alpha = 1$

Method	C_L	C_D	C_M
Pulliam [12]	0.3938	0.0604	-0.1393
Zhou & Davidson [9]	0.3890	0.0662	-0.1282
Dervieux & Debiez [13]	0.3520	0.0418	-
Jameson & Martinelli [14]	0.3861	0.0582	-
SBIC(C grid)	0.3700	0.0576	-0.1166
SBIC(H grid)[11]	0.331	0.0584	-0.119

Table 3. Aerodynamic coefficients NACA0012 $M = 0.8$, $\alpha = 1.25$

Method	CL	CD	CM
Rizzi [8]	0.3513	0.023	-0.0377
Caughey [15]	0.3695	0.0237	-0.0432
Pulliam [12]	0.3618	0.0236	-0.0411
Zhou & Davidson [9]	0.3575	0.022	-0.0375
Jameson & Martinelli[14]	0.3654	0.0232	-
SBIC(C grid)	0.3281	0.0255	-0.0320
SBIC(H grid)[11]	0.334	0.025	-0.041